

Proposal: LTP-9-8

Council: 10/2018

Title: A mobile set-up for simultaneous and in situ neutron reflectivity, infrared spectroscopy, and ellipsometry studies

Research area:

This proposal is a new proposal

Main proposer: Reiner DAHINT

Experimental team: Thomas EDERTH
 Bela NAGY
 Samantha MICCIULLA
 Christian BUSCH
 Reiner DAHINT
 Andreas STOCKLIN

Local contacts: Philipp GUTFREUND
 Samantha MICCIULLA

Samples: Phospholipids
 silicon block
 gold nanoparticles
 Neutral polymer for hydrogel formation
 Zwitterionic polymer
 Metal oxide nanoparticles
 Lipid-coated silicon block (Si)
 Si block with thin polymer film (elements C, H, D, N in different ratios)

Instrument	Requested days	Allocated days	From	To
FIGARO	12	12	18/02/2020	21/02/2020
			22/09/2020	25/09/2020
			25/06/2021	28/06/2021
			04/10/2021	07/10/2021
D17	6	6	22/06/2021	25/06/2021
			01/10/2021	04/10/2021

Abstract:

Neutron reflectivity (NR) is a non-destructive technique for detailed analysis of layered structures on molecular length scales providing thickness, density, roughness and composition of individual layers or components of adsorbed films. However, information on specific molecular groups or their conformation is not accessible. Moreover, NR cannot determine large layer thicknesses, and its time resolution is limited, making it challenging to resolve the kinetics of fast surface processes. The goal of this proposal is to implement an integrated portable sample environment for simultaneous in situ characterization including (i) NR for structural analysis, (ii) infrared spectroscopy in total reflection geometry (ATR-IR) for the determination of molecular entities and their conformation, and (iii) spectroscopic ellipsometry (SE) for rapid and independent measurement of layer thicknesses. The high potential of this approach will be shown by studying (i) the impact of metal and metal oxide nanoparticles on lipid membranes and membrane proteins, to identify potential mechanisms of nanotoxicity, and (ii) the pH-dependent swelling and tunable protein resistance of polyelectrolyte layers.

Experimental report LTP-9-8

Reiner Dahint,¹ Christian Busch,¹ Bela Nagy,² Andreas Stöcklin,¹ Philipp Gutfreund,³ and Thomas Ederth²

¹ *Applied Physical Chemistry, Institute for Physical Chemistry, Heidelberg University, Im Neuenheimer Feld 253, 69120 Heidelberg, Germany*

² *Division of Biophysics and Bioengineering, Dept. of Physics, Chemistry and Biology (IFM), Linköping University, 581 83 Linköping, Sweden*

³ *Institut Laue-Langevin, 71 Avenue des Martyrs, CS 20156, 38042 Grenoble Cedex 9, France*

1. Introduction and aim of the project

Many challenges in science and society concern phenomena that are governed by processes at interfaces, for example, the interaction of drugs and other objects with cell membranes, the compatibility of artificial materials with blood and tissue, catalytic processes for energy conversion or pollution reduction, coatings for anticorrosion or lubrication, and atmospheric processes. Modern surface chemistry concerns understanding and control of surface reactions and processes at the molecular level, and its role in shaping modern society is hard to overestimate. However, for complex interfaces, we still lack combined *in situ* data on structure, kinetics and composition which is required for rational design of functional coatings.

Neutron reflectometry (NR) offers unique opportunities in resolving structure-function relationships of interfacial layers that play a prominent role in soft matter science, biophysics and biomedicine. It is a non-destructive technique for detailed analysis of layered structures on molecular length scales due to short wavelengths and deep penetration of neutrons. Accessible parameters are the thickness, density, roughness and composition of individual layers or components of adsorbed films. In contrast to optics, film density and thickness can be disentangled even for thin layers. However, identification of specific molecular groups or their conformation is not accessible, but this information would significantly help to derive a complete picture of interfacial properties. Moreover, NR cannot determine large layer thicknesses, and the time resolution is limited, making it challenging to resolve the kinetics of fast surface processes.

The goal of this project was to design and implement an integrated sample environment for *in situ* characterization including (i) neutrons for structural analysis, (ii) infrared (IR) spectroscopy in attenuated total reflection geometry (ATR-IR) for the determination of molecular entities and their conformation, and (iii) spectroscopic ellipsometry (SE) for rapid and independent measurement of adsorbate layer thicknesses and refractive indices. It should be possible to use these techniques simultaneously, in various combinations, or independently. Moreover, it is essential that the equipment is portable, so that it can be brought from the home laboratories to beamlines or exchanged between reflectometers with little effort, increasing its use and availability for a broad scientific community. The optical techniques may in principle also be combined with X-ray reflectometry (XRR) instead of NR. The performance of the new set-up was tested and demonstrated within the framework of two scientific pilot projects, which were (i) the impact of metal and metal oxide nanoparticles on lipid membranes and membrane proteins to identify potential mechanisms of nanotoxicity, and (ii) the pH-dependent swelling and tunable protein resistance of polyelectrolyte layers.

2. Progress report 2020

Beamtimes

FIGARO 18.02.2020 – 21.02.2020

FIGARO 22.09.2020 – 25.09.2020

2.1 Experimental setup

The ATR-IR setup, developed at Heidelberg University, is based on a modular Nicolet iG50 Fourier-Transform IR spectrometer. It covers a spectral range from 720 cm^{-1} to 4000 cm^{-1} . Resolution can be selected between 0.125 and 32 cm^{-1} . Accordingly, the time required for one complete scan ranges from about 5.7 to 0.3 s.

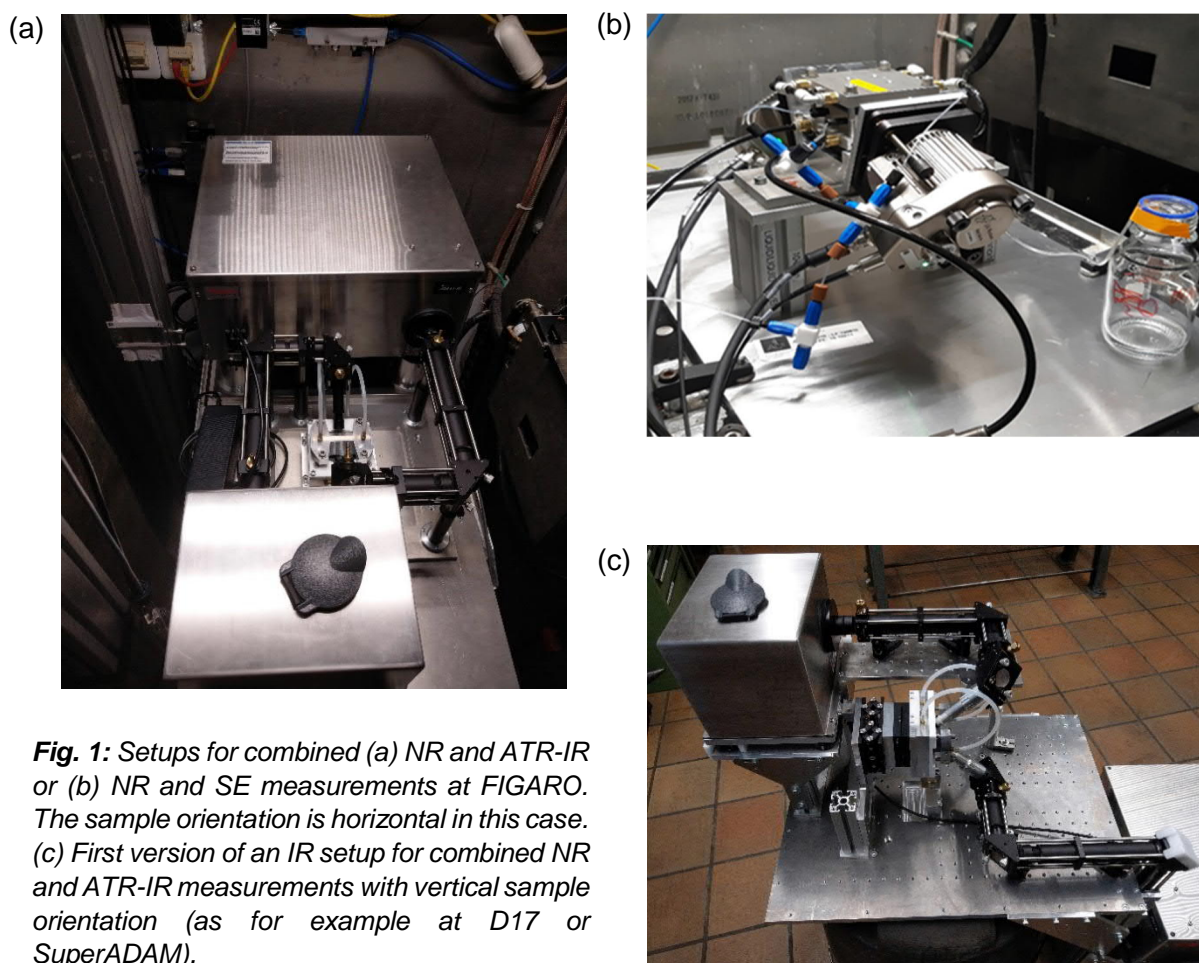


Fig. 1: Setups for combined (a) NR and ATR-IR or (b) NR and SE measurements at FIGARO. The sample orientation is horizontal in this case. (c) First version of an IR setup for combined NR and ATR-IR measurements with vertical sample orientation (as for example at D17 or SuperADAM).

As already described in the report for experiment TEST-3045, a first version of the setup was brought to ILL during a reactor shutdown in August 2019, provisionally mounted on the sample stage of the neutron reflectometer FIGARO and adapted to the conditions on site. As future IR measurements were to be performed in aqueous media, an ATR geometry was selected. Based on the knowledge gained, the optical beam path and the stability of the setup were optimized, and the assembly of the apparatus was simplified. In February 2020, it was used for the first time for combined NR and ATR-IR measurements at FIGARO (Figure 1a). The experiments performed are described in section 2.2. In order to be able to conduct combined NR and IR measurements also with vertical sample orientation as it is the case, for example, at the neutron reflectometers D17 and SuperADAM, a second ATR-IR setup was developed

and successfully tested in Heidelberg, which is adapted to the corresponding conditions (Figure 1c).

In parallel, the development of an apparatus for combined NR and SE measurements has been continued at Linköping University (Figure 1b). The ellipsometric function is built around a modular J. A. Woollam iSE spectroscopic ellipsometer with dual rotating compensators, forming a PCSCA (polarizer-compensator-sample-compensator-analyser) configuration. It covers 190 wavelengths from 400 nm to 1000 nm, and completes a measurement of the entire spectral range within 0.3 - 2 s. Special attention was paid to the compatibility of the developed components with the ATR-IR setup in order to enable the integration of both measurement setups in a next step. First combined NR and SE measurements were performed at FIGARO in September 2020. The results are presented in section 2.3.

2.2 Interaction of nanoparticles with lipid films

In the last decade, metal and metal oxide nanoparticles (NPs) have found increasing use in biomedical applications and consumer products. Therefore, the question arises whether they may pose risks to human health. Indeed, several studies suggest that the interaction of NPs with cell membranes may affect cell function and contribute to toxic effects. In addition to *in vivo* studies, model systems based on solid-supported lipid membranes play an important role in the study of such processes, as individual experimental parameters can be specifically modified. Previous studies have shown that, in particular, the charge of the NPs, their hydrophilicity, size, shape and chemical composition, as well as the phase state of the lipid membranes (gel-like or liquid crystalline) significantly affect these interactions. However, a detailed understanding of the underlying processes at the molecular level has not yet been achieved.

In combined NR and ATR-IR measurements at FIGARO we investigated how NPs of different size and composition interact with lipid oligobilayers of DMPC (1,2-dimyristoyl-sn-glycero-3-phosphocholine). DMPC differs from 1,2-dipalmitoyl-sn-glycero-3-phosphocholine (DPPC), one of the most abundant lipids in human cells, only by a two carbon atoms shorter alkyl chain, but has a lower main phase transition temperature T_M , which was advantageous for some of our experiments (*cf.* section 3.2). Lipid films were prepared on silicon ATR crystals by spincoating. The use of oligobilayers – instead of single bilayers – not only amplifies the signal, but also minimizes potential spurious lipid/substrate interactions for all bilayers except the one which is in direct contact with the crystal. The accessibility of the lower bilayers to the NP solution is provided by defects in the layer system. The lipid films were prepared with a cholesterol content of 20 and 30%, respectively, corresponding to typical conditions in biological cells. They were first measured against D₂O and then against a 50 mM MgCl₂ solution in D₂O. In the latter case, the ionic strength of the solution was similar to that of an isotonic saline solution.

As shown by the NR measurements, the change from D₂O to a 50 mM MgCl₂ solution resulted in a significant increase in the interfacial water layer thickness between individual bilayers in the case of DMPC films containing 20% cholesterol (Figure 2). The total number of bilayers decreased slightly. When fitting the NR data, it became apparent that they could only be satisfactorily fitted using an incoherent model in which the scattering of intact film regions is superimposed on that of hole regions. Atomic force microscopy (AFM) measurements on DMPC oligobilayers performed in ambient air confirmed that larger holes are formed when

cholesterol is added. Their dimensions exceed the coherence length of the neutron beam for higher values of the wave vector transfer Q .

The addition of gold NPs (AuNPs, 2 or 5 nm in size, concentration 10 or 40 $\mu\text{g}/\text{mL}$, respectively) resulted in a further slight increase of the interfacial water layer thickness for films containing 20% cholesterol. This effect is enhanced at higher AuNP concentration. In addition, the total number of bilayers decreased with increasing AuNP content. The behavior observed in the NR experiments was also reflected in the ATR-IR measurements (Figure 3): Due to the exponentially decreasing electric field in ATR configuration, the intensity of the symmetric and anti-symmetric CH_2 stretching bands decreased with swelling processes, i.e., increasing distance of the molecules from the surface. In addition, the strength of the bands decreased upon loss of bilayers. The IR band position proved that the films were in the gel-like P_{β} phase.

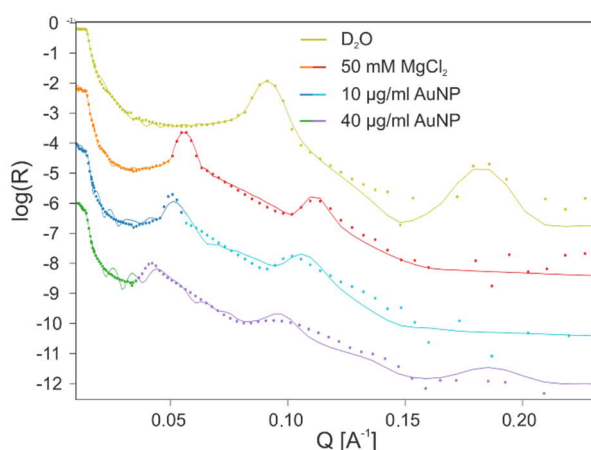


Fig. 2: NR measurements on FIGARO on the influence of MgCl_2 and AuNP solutions on lipid oligobilayers. The measurements shown here were performed on a DMPC film containing 20% cholesterol. The AuNP solutions contained 50 mM MgCl_2 , and the size of the AuNP was 2 nm. For $Q < 0.05 \text{ \AA}^{-1}$, data were fitted with a coherent, and for higher values of Q with an incoherent model.

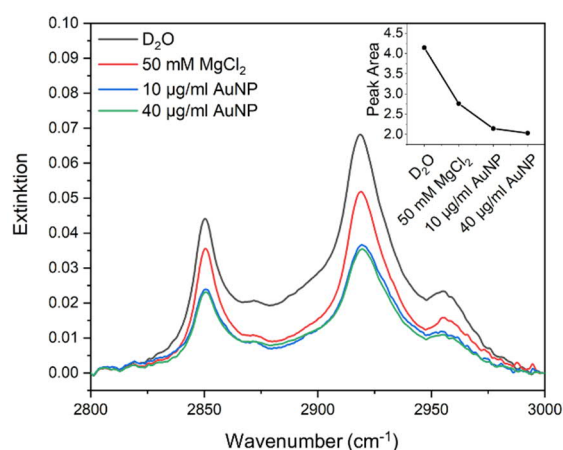


Fig. 3: Parallel ATR-IR measurements on the systems displayed in Fig. 2. Shown is the region of the symmetric and anti-symmetric CH_2 stretching bands. The decrease in peak intensity is due to both stronger swelling of the films and loss of individual bilayers. This effect might be mitigated by CH_2 groups associated with the ligands of bound AuNP.

In contrast, the addition of titanium oxide NPs resulted in only a comparatively moderate increase in the equilibrium distance between adjacent bilayers. The total number of lipid bilayers did not change upon titanium oxide NP addition. This is consistent with SE measurements, where titanium oxide NP addition also did not result in any measurable changes in the total thickness of the lipid oligobilayers.

For the films containing 30% cholesterol, the addition of AuNPs (also 2 and 5 nm in size, concentration 10 and 40 $\mu\text{g}/\text{mL}$, respectively) also increased equilibrium distances of the lipid bilayers slightly. However, in this case the total number of layers remained constant. Cholesterol thus appears to exert a stabilizing effect on the films and reduce NP-induced damage. SE measurements further showed that when iron oxide NP solutions were added, only the lipid bilayer directly attached to substrate remained and all other layers were lost.

Supplementary measurements by SE, quartz crystal microbalance with dissipation monitoring (QCM-D), IR spectroscopy and X-ray reflectometry (XRR) largely support the above results.

2.3 pH-induced swelling of polyelectrolyte layers

In initial combined NR and SE measurements, the structure of poly(2-hydroxyethyl methacrylate-co-poly(ethylene glycol) methacrylate) (poly(HEMA-co-PEGMA)) was studied under water. Different mixtures of D₂O and H₂O were used to vary the scattering length density (SLD) of the bulk phase. Prior to the measurements, the sample mounted in the liquid flow cell was purged with dry gaseous nitrogen to determine the amount of immobilized polymer from the dry film thickness. Figure 4 shows the ellipsometrically determined change in film thickness during the drying process.

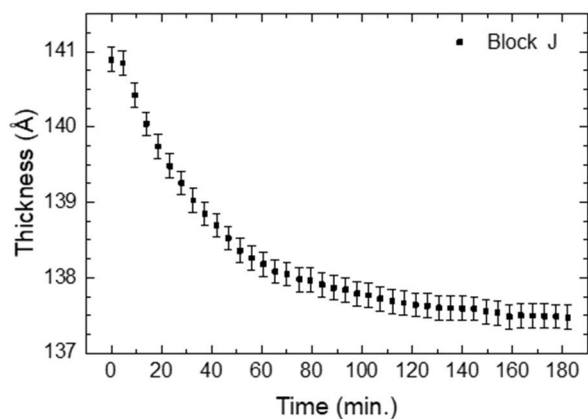


Fig. 4: First measurements with the combined NR/SE setup. The SE signal shows the layer thickness decrease of the poly(HEMA-co-PEGMA) film when rinsed with dry gaseous nitrogen at the beginning of the measurement.

For the measurements in aqueous environment, the parallel acquisition of NR and SE data was successfully demonstrated. However, the test also revealed some weaknesses in the flow system. Inadvertent bubble formation and inefficient fluid exchange occurred, although the latter had been verified and optimized prior to the experiment in the home laboratory at Linköping University using different configurations of the fluid cell with stained water and a dummy glass block. However, the density differences in waters of different D₂O/H₂O contrasts had not been taken into account, and apparently reduced the exchange performance. The fluid exchange problems were primarily reflected in temporal changes in the SE signal. These were not apparent in the NR measurements, as the comparatively small variations in mixing were averaged out by the – compared to SE measurements – significantly longer data acquisition time. The issue of density differences has been taken into account in subsequent designs of the flow cell.

The accidental entering of bubbles into the flow system could be largely prevented by an external bubble trap. However, we also realized that it might be desired to use slightly different flow path designs in order to minimize these problems from the outset. The plan to fabricate flow cells in stainless steel was discarded as cells made of PEEK have a similar neutron scattering background and also offer much better possibilities of making fine details in the flow paths at a reasonable time and cost. Awaiting further beamtime, efforts have been directed to developments which were not initially planned for, such as an SE setup facilitating a sample translator for experiments on multiple samples in sequence, preparing for experiments with a rapid sample turnover, as expected for the FREIA and ESTIA beamlines under construction at the ESS, and integration of the pump/fluidic system with ellipsometric measurements to automatize monitoring of liquid sample changes.

3. Progress report 2021

Beamtimes

D17	22.06.2021 – 25.06.2021
FIGARO	25.06.2021 – 28.06.2021
D17	01.10.2021 – 04.10.2021
FIGARO	04.10.2021 – 07.10.2021

3.1 Experimental setup

Work in the reporting period focused primarily on combining *in situ* NR, ATR-IR, and SE in a setup that allows for the simultaneous use of all three techniques. In the year before, the combination of two investigation methods at a time – NR and ATR-IR, or NR and SE – had been successfully demonstrated in separate experiments. Figure 5 shows engineering drawings of the mobile component of the newly developed setup for horizontal and vertical sample orientation. The flow cell with the mounted film-coated ATR crystal, the optical components of the ATR-IR beam path and the two ellipsometer heads with radiation source and detector, respectively, can be seen in central position. The actual setups installed on FIGARO and D17 are displayed in Figure 6.

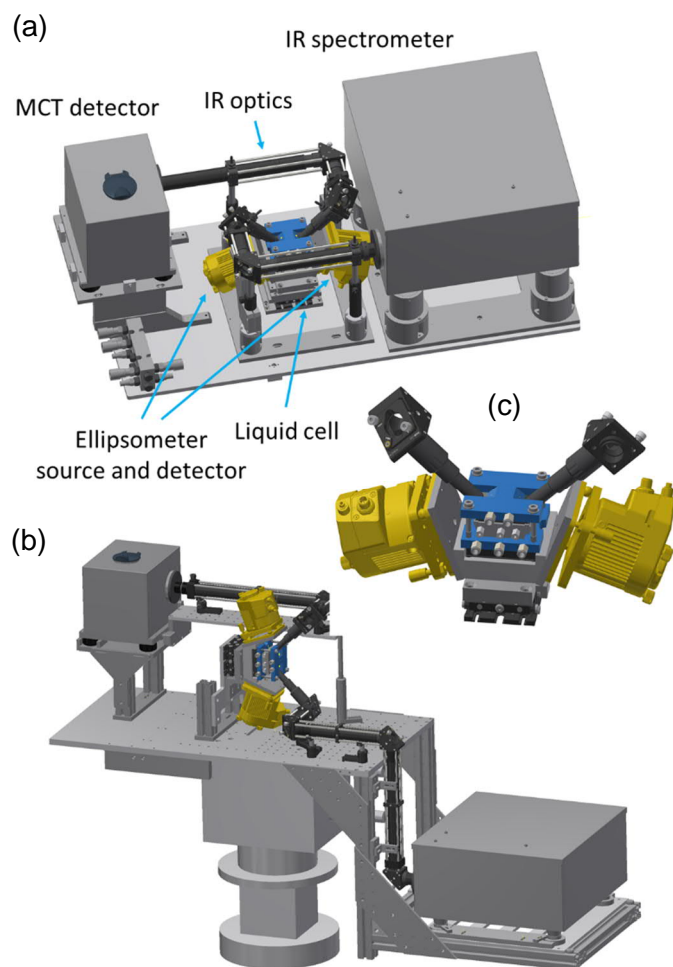


Fig. 5: Setups for parallel NR, ATR-IR and SE measurements, including designs for horizontal (a) and vertical (b) sample orientation. The ellipsometer source and detector units are indicated in yellow, and the liquid flow cell assembly in blue. (c) Close-up of the liquid cell and the ATR crystal interfaced to the IR and ellipsometry pathways.

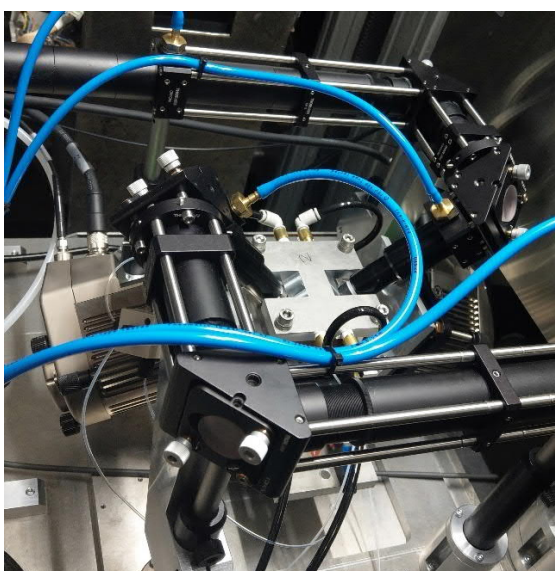
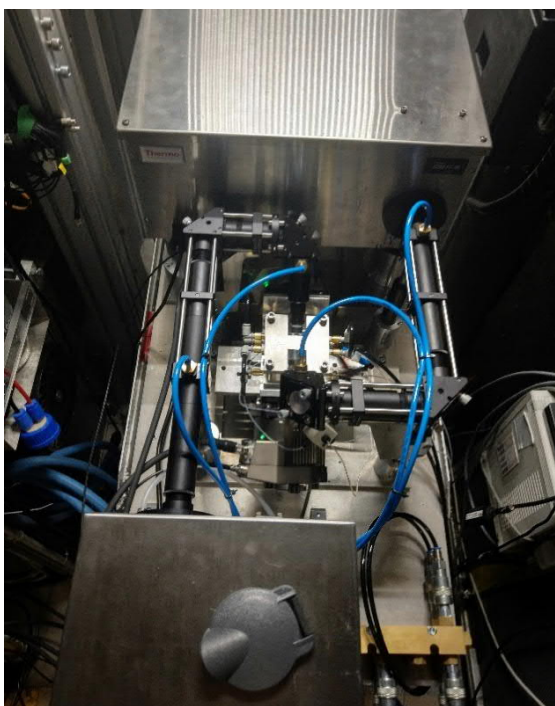


Fig. 6: Installation of the mobile ATR-IR/SE setup on FIGARO (left) and D17 (right). The lower two photos each show a magnified view of the liquid flow cell with IR beam path, and SE light source and detector, respectively.

Key aspects of the liquid flow cell design were the opportunity to fill it without bubbles, to allow for effective liquid exchange (Figure 7), and to provide the spatial conditions for simultaneous assembly of ATR-IR and SE components. Especially for ellipsometric measurements the former aspect is of high relevance, since bubbles in the beam path massively disturb the signal. Effective fluid exchange is essential for carrying out measurement series without dismantling the flow cell and readjusting the setup. Especially with regard to automated measurements and optimization of neutron beam time, this is an important feature.

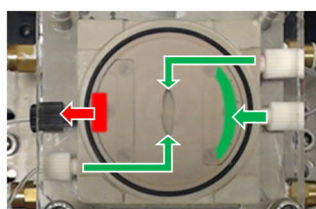
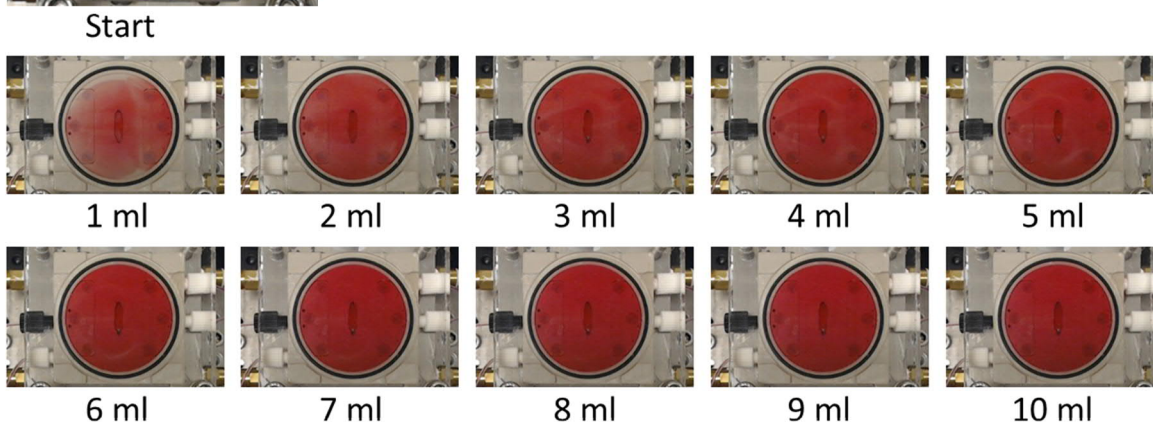


Fig. 7: Exchange of D_2O with stained H_2O in the liquid cell at a flow rate of 1 ml/min. The top figure shows the inlet (green) and outlet (red) channels of the flow cell. After approximately 10 ml of flow, a complete liquid exchange is achieved. Increasing the flow rate to 5 ml/min does not result in any visible change.



The two versions of the setup have been successfully combined and tested with the neutron reflectometers FIGARO (horizontal sample orientation) and D17 (vertical sample orientation). Related experiments are described in chapters 3.2 and 3.3. Furthermore, it has been shown that the setup for vertical sample orientation can also be adapted to SuperADAM. Thus, we have succeeded in developing a setup for simultaneous NR, ATR-IR, and SE studies which is mobile and can be flexibly used on different neutron reflectometers. The instrumental goals of the research project have, therefore, been fully achieved. A publication on the new experimental setup including proof-of principle experiments has been submitted for publication in August 2022.

3.2 Interaction of nanoparticles with lipid films and membrane proteins

Simultaneous NR, ATR-IR and SE measurements were used to investigate the interaction of AuNPs with DMPC oligobilayers at temperatures below and above the main phase transition temperature T_M . Again, the films were prepared by spincoating. Figure 8a shows the neutron reflectance of DMPC oligobilayers exposed to D_2O at 18 and 26 °C, i.e., at temperatures well below and above $T_M \approx 24.2$ °C. The main differences between the film structures are the reduced lipid chain length, the increased area per molecule, and the significant reduction of water content in the lipid layers at higher temperatures. While the first two features are consistent with a transition from the gel-like P_{β} phase to the liquid crystalline L_{α} phase, the latter indicates an annealing process resulting in more compact lipid films with fewer water inclusions. The improved packing after annealing at higher temperatures has been confirmed by AFM measurements on DMPC oligobilayers performed in ambient air.

The addition of AuNPs with a diameter of about 50 nm leads to a successive degradation of the lipid films as shown by the decrease in the Bragg peak (see inset in Figure 8a, measured data shown as lines). The reduction of film thickness derived from the NR data is displayed in Figure 9. In the following, the time interval Δt_{50} from the beginning of film degradation to the time when 50% of the total film thickness has been lost, is used as a measure of film stability. As can be seen from Figure 9, the degradation of the lipid layers in the L_{α} phase is significantly faster than in the P_{β} phase.

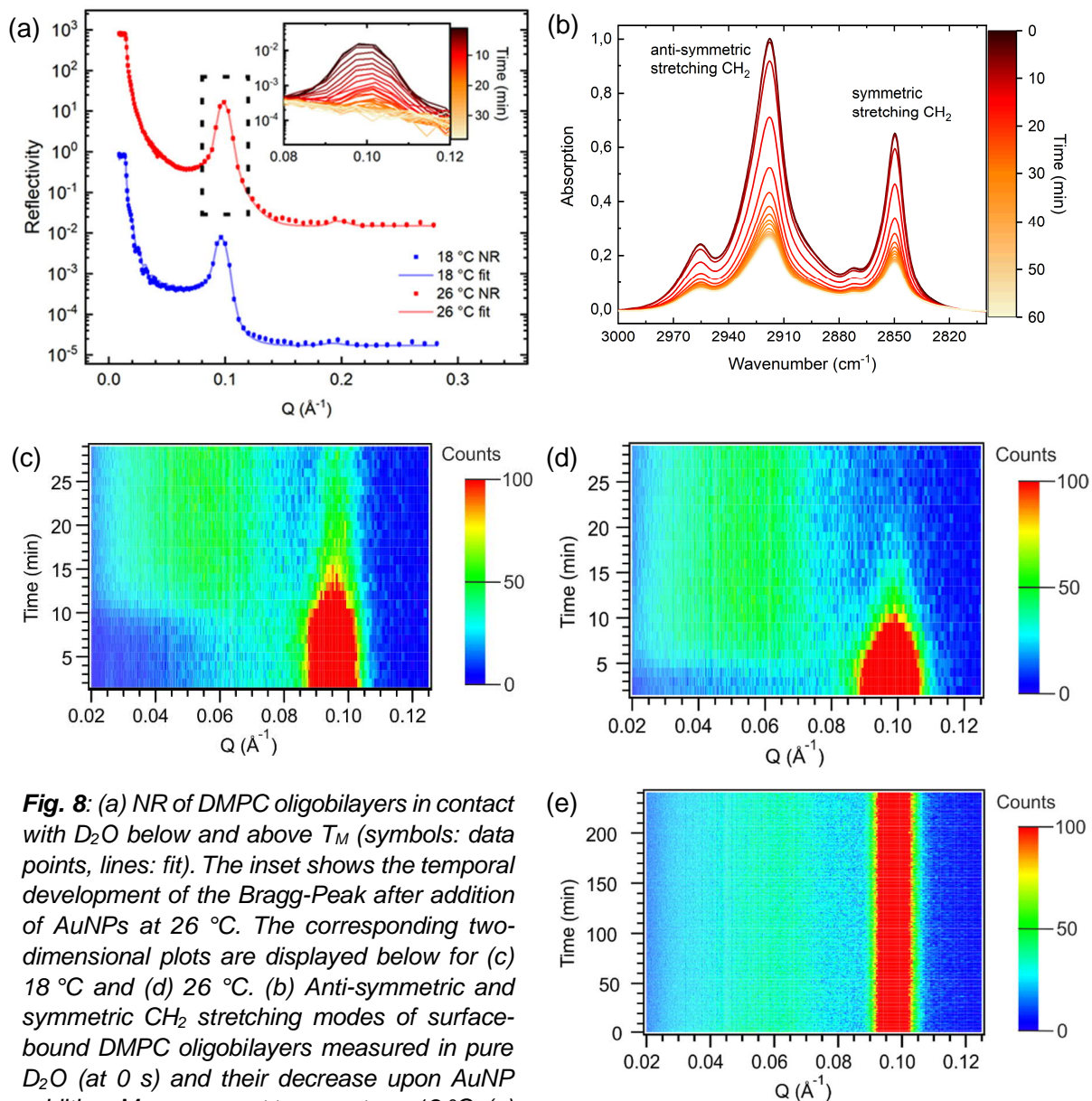


Fig. 8: (a) NR of DMPC oligobilayers in contact with D_2O below and above T_M (symbols: data points, lines: fit). The inset shows the temporal development of the Bragg-Peak after addition of AuNPs at 26 °C. The corresponding two-dimensional plots are displayed below for (c) 18 °C and (d) 26 °C. (b) Anti-symmetric and symmetric CH_2 stretching modes of surface-bound DMPC oligobilayers measured in pure D_2O (at 0 s) and their decrease upon AuNP addition. Measurement temperature: 18 °C. (e) NR of oligobilayers composed of 70% DMPC and 30% cholesterol in contact with an aqueous AuNP solution at 24.2 °C.

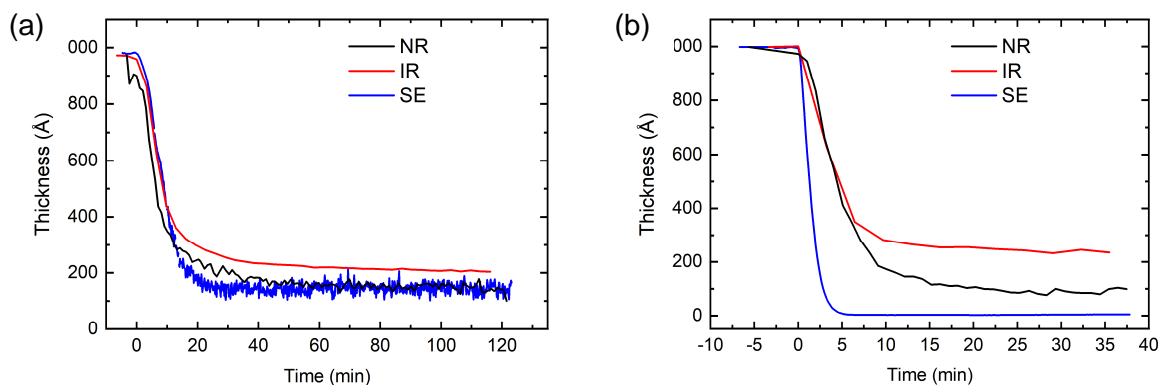


Fig. 9: Degradation of DMPC oligobilayers upon contact with AuNPs determined simultaneously by NR, ATR-IR and SE at (a) 18 and (b) 26 °C. The Δt_{50} values determined are 8.3 (NR), 8.9 (IR) and 9.2 min (SE) at 18 °C and 4.2 (NR), 4.8 (IR) and 1.7 min (SE) at 26 °C.

The successive degradation of the lipid layers can also be observed in simultaneous ATR-IR measurements based on the decrease of the symmetric and anti-symmetric CH_2 stretching modes (see Fig. 8b), and by SE. In the evaluation of the IR data, the exponential decay of the electric field at the solid/liquid interface was taken into account. All experimental techniques applied consistently show a faster degradation of the films above the main phase transition temperature (see Figure 9). Except for the SE measurement at 26 °C, all Δt_{50} values at a given temperature lie in a close range. We suspect that the small difference in refractive index between the water containing DMPC oligobilayers and the bulk water phase may be the reason for the observed deviation. While at 18 °C the final film thickness is very similar, some deviation is observed at 26 °C depending on the technique used. The reason for this behavior is still being investigated. Again, incorporation of cholesterol significantly stabilized the lipid layers. For films prepared from mixtures of 70% DMPC and 30% cholesterol no degradation was observed upon AuNP contact even for elevated temperatures (Figure 8e).

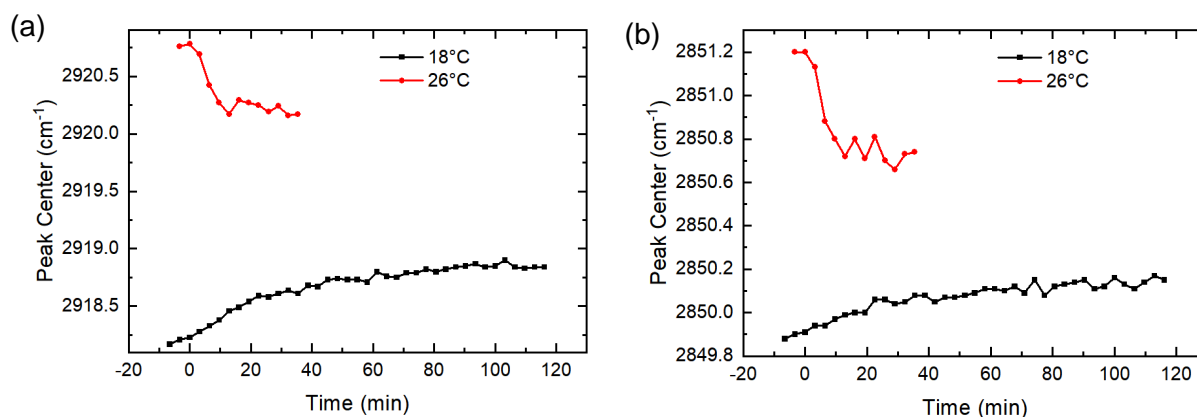


Fig. 10: Shift of the peak position of the (a) anti-symmetric and (b) symmetric CH_2 stretching mode upon AuNP addition.

In the L_α phase, the position of the CH_2 stretching modes is about 1.5 (symmetric mode) to 2.5 cm^{-1} (anti-symmetric mode) higher than in the P_β phase (*cf.* starting time $t=0$ in Figure 10), which also allows to control the phase state of the films. Based on the observation that the difference in band position is reduced with increasing AuNP incubation time (Figure 10), one may conclude, that the structural features of the lipid oligobilayers become more similar upon NP interaction.

In subsequent experiments, the interaction of AuNPs with integral and peripheral membrane proteins was to be investigated. Cytochrome C served as an example of a peripheral protein and gramicidin as a model integral protein. For cytochrome C the idea was to adsorb it onto DMPC oligobilayers from aqueous solution as described in literature. However, no distinct changes in the NR curves upon protein solution contact were observed and also no amide bands showed up in the ATR-IR spectra indicating that no significant amount of protein had adsorbed to the lipid films.

In case of gramicidin, mixtures of protein and DMPC or protein, DMPC and cholesterol were spincoated onto the substrates. Figure 11 shows experiments where 10% gramicidin have been added to a lipid solution containing 80% DMPC and 20% cholesterol prior to spincoating. To fit the NR data, an incoherent model was used in which it was assumed that the films consist of two types of areas with different numbers of bilayers (Figure 11a). The gramicidin content caused a higher SLD and slightly smaller film thickness in the tail group region, while the head group region remained mostly unaffected compared to films without protein content. Addition

of 2 nm AuNPs did not result in any change in film structure. Observed variations in the peak area of the amide I band can be attributed to variations in the H₂O rotational bands originating from traces of moisture in the optical system. Further addition of 50 nm AuNPs led to an increase in tail group thickness with a simultaneous decrease in interfacial water layer thickness. However, no change in the ATR-IR spectra was observed.

Addition of MgCl₂ to obtain a 50 mM aqueous solution resulted in a swelling of the lipid film by a factor of 2.3. This effect was also observable in the IR spectra in form of decreasing intensities of the CH₂ stretching and amide I bands due to the exponential decay of the electric field at the solid/liquid interface (Figure 11b). However, no change in the shape of the amide I bands could be detected, which would suggest a change in the secondary structure of the protein. A subsequent temperature increase caused further swelling of the system (Figure 11c). Fitting of the NR data is still ongoing. While the amide I bands remained unaffected, except the expected reduction in peak area, the CH₂ stretching bands showed a shift towards larger wavenumbers, indicating structural changes in the lipid films (Figure 11d).

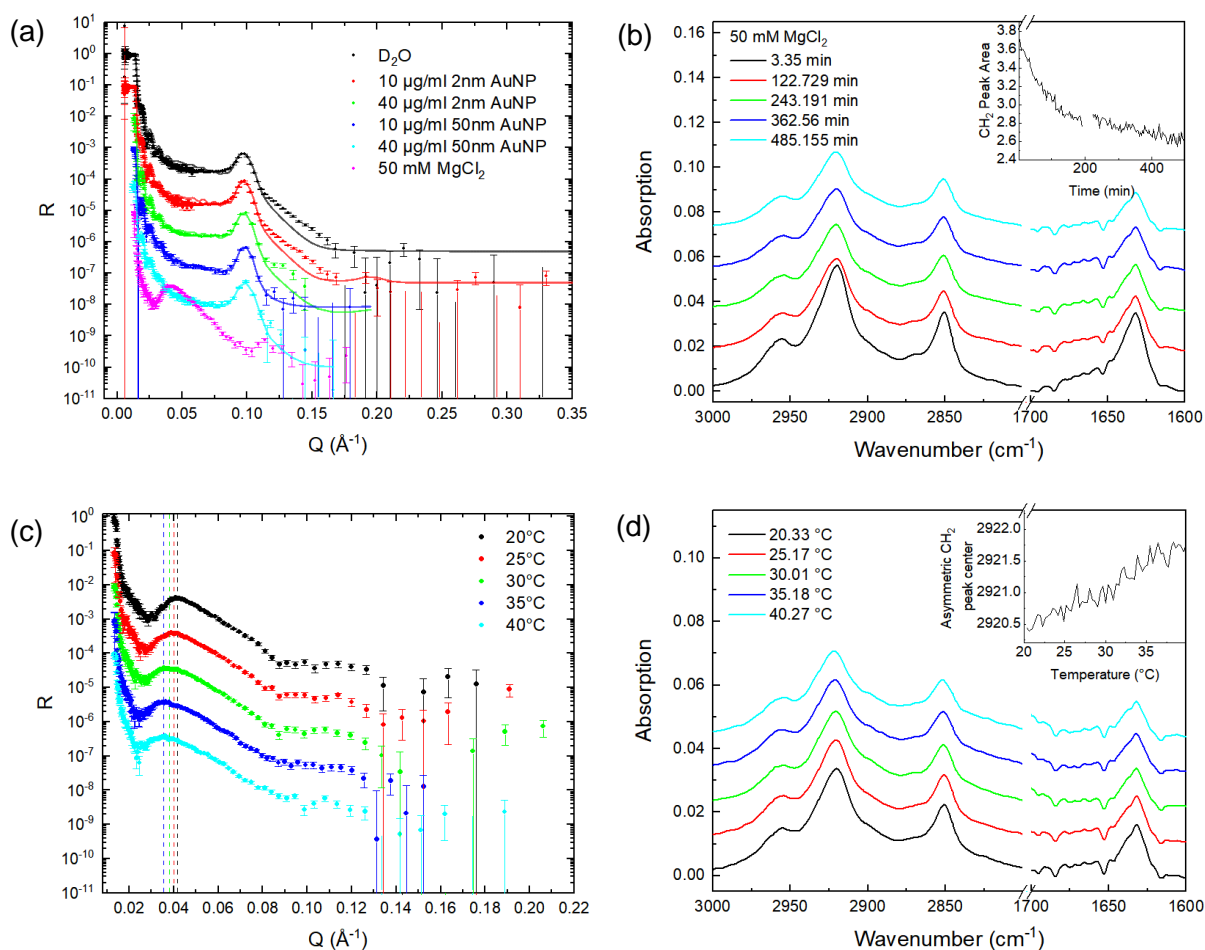


Fig. 11: Experiments on lipid oligobilayers with integrated gramicidin. (a) NR of the films in contact with D_2O and aqueous AuNP and $MgCl_2$ solutions (symbols: data points, lines: fit). (b) Temporal change of the ATR-IR spectra after addition of 50 mM $MgCl_2$ solution. (c) NR at different temperatures and (d) corresponding ATR-IR spectra.

3.3 pH-induced swelling of polyelectrolyte layers

Polyelectrolyte films containing both cationic and anionic ionizable residues (polyampholytes) allow for tuning the structure, swelling, and the antifouling properties of the films via variations in composition, structure, pK_a / pK_b of the ionizable residues, solution salinity or pH. While the structure and properties of polyampholytes remain important targets of study, less complex single-component polyelectrolyte films were used to explore the capabilities of the new setup, namely anionic poly(methacrylic acid) (pMMA) and cationic poly(2-dimethylaminoethyl methacrylate) (pDMAEMA). Measurements were performed at three different solvent contrasts: D_2O , CM3 (50:50 $D_2O:H_2O$), and H_2O . Each sample was further measured in aqueous solutions of HCl and NaOH, respectively, at pH values of approximately 3.1 and 12.7 as measured in H_2O . The NR data from the polymers were fitted to a model consisting of three slabs with sigmoidal interfacial roughnesses, corresponding to the Si/SiO₂/silane layers, an additional slab for the interface between the polymer and the silane layers and a polymer layer that was modelled using a sliced sigmoidal volume fraction profile. NR data from the pDMAEMA film are shown in Figure 12a. The resulting density profiles of the polymer chain segments in Figure 12b clearly show the response of the cationic polyelectrolyte to changes in pH. At low pH, the tertiary amines are protonated and the polymer is stretched due to charge-charge repulsion within the polymer. At a high pH, deprotonation leads to a collapse of the layer. However, this collapse is not complete as some water is still trapped in the film.

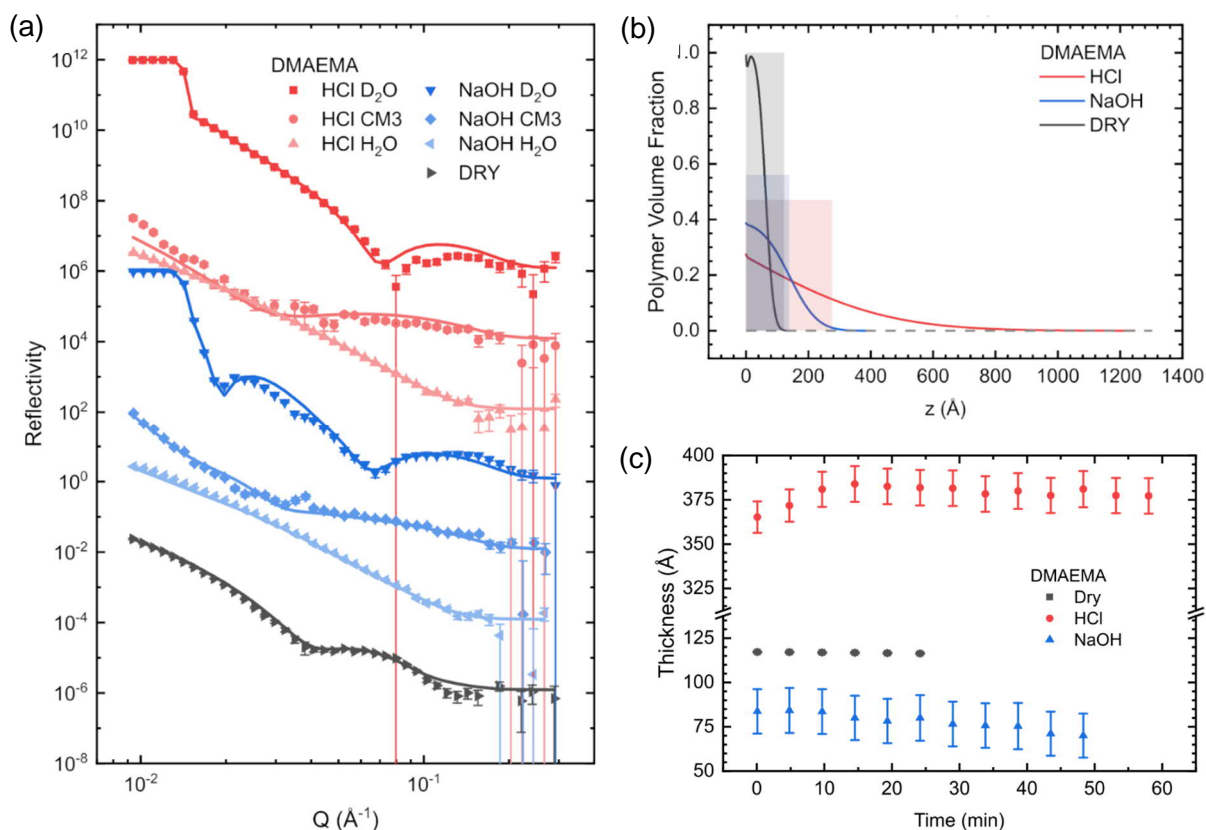


Fig. 12: (a) NR data (symbols) and corresponding fits (lines) for a pDMAEMA film at three different contrasts and two pH values each. The data set for the dry film (black symbols, bottom) is correctly positioned on the vertical axis, subsequent data sets have been scaled $\times 100$ relative to the previous data set for clarity. (b) Polymer volume fraction profiles according to the fit results from (a). The rectangles show the thickness and volume fractions as obtained from parallel SE measurements. (c) Ellipsometrically determined time evolution of the film thickness after pH change or removal of water from the system.

The rate of these processes cannot be followed with NR, but SE data show that swelling and collapse proceed at different rates (Figure 12c). Swelling after addition of HCl is relatively fast and reaches a plateau after about 10 min. Collapse after addition of NaOH is slower and is accompanied by a slow decrease in thickness and a corresponding increase in polymer volume fraction within the layer. The slower equilibrium in the latter case is probably an effect of hindered water diffusion upon compression of the polymer. A comparison of the ellipsometric thicknesses and volume fractions with the fitted NR data reveals clear differences for the hydrated films (Figure 12b). The volume fractions for the hydrated films are relatively similar, but the thicknesses are not. We interpret this as a difference in sensitivity to the location of the diffuse polymer/water interface, where the uncertainty lies primarily in the ellipsometric measurement because the optical contrast between bulk water and the film is very low and cannot be adjusted by isotope selection as in NR. These differences and the potential for co-fitting of NR and SE data are the subject of ongoing studies.

The characteristic IR bands of amines are generally very weak, and the spectral features of tertiary amines, such as DMAEMA, are particularly featureless in the absence of N-H stretching modes. Therefore, the results of the IR spectra of the pMAA films are shown below. For each polymer film sample, IR background spectra were obtained with the film hydrated with 10 mM HCl in D₂O, and all spectra show differences in relation to this state. IR spectra obtained at the same pH but different contrasts show effects of bulk liquid exchange (Figure 13a). In H₂O, the broad O-H stretching mode emerges around 3600 - 3000 cm⁻¹, as well as the H-O-H bending mode near 1600 cm⁻¹ and the corresponding bands for the displaced deuterated water (O-D and D-O-D) appear as negative bands. The H₂O/D₂O mixture CM3 also contains contributions from these as well but of smaller magnitude than expected, and a new band for the bending mode of the isotopically mixed water molecule H-O-D at about 1500 cm⁻¹.

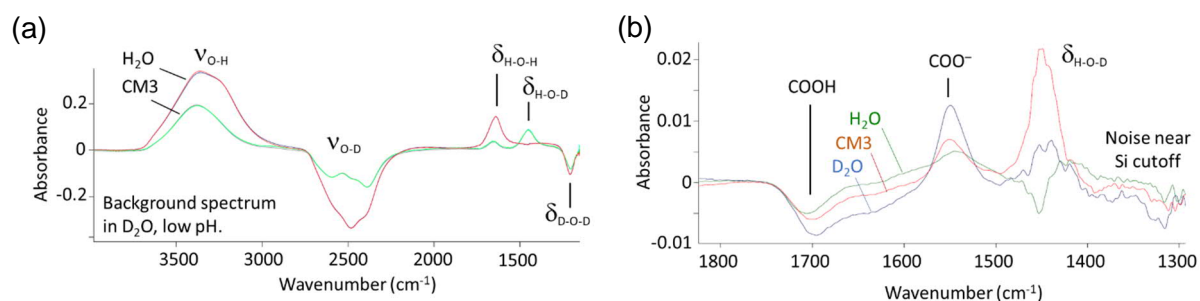


Fig. 13: (a) IR spectra at pH 3.1 in CM3 and H₂O reflect the differences in the bulk phase. (b) Difference between IR spectra at high and low pH for the three different liquid contrasts. The differences in the spectra show the influence of pH on the polymer film.

Comparing instead the difference spectra between similar contrasts but different pH values reveals differences due to variations in the degree of ionization. Figure 13b shows the result for the three contrasts when the pH is changed from 3.1 to 12.7. This change is associated with a deprotonation of the carboxylic acids, which can be observed as a negative band around 1700 cm⁻¹ and an associated increase in the carboxylate ion band at 1550 cm⁻¹. The thickness of the pMAA film studied is only 40 Å in the collapsed dry state, and from the signal-to-noise ratio in Figure 13b it appears that the overall sensitivity of the ATR-IR setup is overall good for this type of study, even with a very thin polymer layer. The increasing noise at lower wavenumbers in Figure 13b originates from the cut-off in transmittance of the silicon block, just outside the wavenumber range shown.

4. Summary and conclusion

We have successfully demonstrated that online, *in situ* monitoring of both, IR spectroscopy and SE data during NR experiments is feasible. This was realized with a mobile and modular setup, which allows either of the methods to be used independent of the other two. The instrumental goals of the research project have, therefore, been fully achieved. We have demonstrated the utility of the combined setup in two different soft matter systems, namely the interaction of AuNPs with lipid oligobilayers and the pH-dependent swelling of polyelectrolyte layers, showing how complementary data, such as chemical information and rapid thickness monitoring can be added to the NR data, providing supplementary information, or may be used to support or validate information obtained by NR. The flexibility of the setup has been demonstrated by its implementation at beamlines with both horizontal and vertical sample geometries.